

ORIGINAL RESEARCH PAPER

## Adsorption of ozone molecules on AlP-codoped stanene nanosheet: A density functional theory study

Amirali Abbasi<sup>1,2,3</sup>

<sup>1</sup> Molecular Simulation Laboratory (MSL), Azarbaijan Shahid Madani University, Tabriz, Iran

<sup>2</sup> Computational Nanomaterials Research Group (CNRG), Azarbaijan Shahid Madani University, Tabriz, Iran

<sup>3</sup> Department of Chemistry, Faculty of Basic Sciences, Azarbaijan Shahid Madani University, Tabriz, Iran

Received: 2018-11-23

Accepted: 2019-01-01

Published: 2019-02-01

### ABSTRACT

Density functional theory calculations were carried out to investigate the structural and electronic properties of the adsorption of O<sub>3</sub> molecules on AlP-codoped monolayers to fully exploit the gas sensing capability of these two-dimensional materials. Various adsorption sites of O<sub>3</sub> molecule on the considered nanosheets were examined in detail. The side oxygen atoms of the O<sub>3</sub> molecule strongly bind to the tin atoms, and provide double contacting point between the nanosheet and O<sub>3</sub> molecule. O<sub>3</sub> adsorption on the Al-site of AlP-codoped structure is more favorable in energy than that on the pristine one. AlP-codoped stanene exhibits better semiconductor characteristics because of the band gap opening in the system. The total electron density plots show the charge distribution along the interacting side oxygen and tin atoms, which indicate the formation of chemical bonds between them. This formation of chemical bond was also evidenced by the projected density of states diagrams. The large overlaps between the PDOS spectra of the oxygen and tin atoms show the formation of chemical bonds between these atoms. The charge density difference calculations represent charge accumulation on the adsorbed O<sub>3</sub> molecule. Our results suggest a theoretical basis for AlP-codoped stanene monolayer as efficient candidate for application in gas sensor devices.

**Keywords:** Adsorption; AlP-Codoped Stanene; Band Structure; DFT; Total Electron Density

© 2019 Published by Journal of Nanoanalysis.

### How to cite this article

Abbasi A. Adsorption of ozone molecules on AlP-codoped stanene nanosheet: A density functional theory study. J. Nanoanalysis., 2019; 6(1): 60-71. DOI: 10.22034/jna.2019.664505

## INTRODUCTION

Two-dimensional (2D) materials with atomic thickness, such as planar graphene, boron nitride, and 2D transition metal dichalcogenides (TMDCs) have aroused substantial interests because of their exceptional properties. The discovery of graphene has encouraged numerous scientists to make efforts in the search for the outstanding properties of 2D materials, such as graphene itself [1], silicene [2-4], germanene [5-6], antimonene [7-8], and transition metal dichalcogenides [9-10]. 2D materials exhibit unique electronic, mechanical, chemical, and physical properties because of the particular honeycomb structure [11-14]. Due to these

\* Corresponding Author Email: [a\\_abbasi@azaruniv.ac.ir](mailto:a_abbasi@azaruniv.ac.ir)

outstanding characteristics, scientists have paid significant attention on exploration of the unique properties of 2D planar structures. 2D structures can be utilized for various applications such as energy conversion or storage photocatalyst [18-19] and nanoelectronic devices [20-23]. Recently, a new 2D layered material, namely stanene has triggered great interests. Stanene also exhibits excellent properties such as Dirac-cone-shaped energy band structure, ultra-high carrier mobility, and unfortunate zero-band-gap nature. Zhu et al. have suggested the experimental synthesis of two-dimensional stanene using molecular beam epitaxy growth on Bi<sub>2</sub>Te<sub>3</sub> (111) substrate [24]. Gao et al.



This work is licensed under the Creative Commons Attribution 4.0 International License.

To view a copy of this license, visit <http://creativecommons.org/licenses/by/4.0/>.

also suggested that monolayer stanene could also epitaxially grow on Ag (111) substrate [25]. Stanene is a zero band gap material without inclusion spin-orbit coupling (SOC) effect. By including spin-orbit coupling, stanene gains a band gap of about 0.1 eV after relaxation [26], which indicates its potential applicability for future optoelectronic devices. Sensing gas molecules such as ozone is a fundamental step in the process of environmental protection, industrial monitoring and medical treatment. Sensitive solid-state gas sensors used for environmental pollution monitoring and agricultural and medical applications have triggered numerous interests. Sensors fabricated based on 2D graphene [27, 28],  $MoS_2$  [29], and phosphorene [30, 31] have been extensively utilized for gas sensing applications because of their low noise and low power consumption. The performance of the gas sensors is restricted by some intrinsic defects, such as low carrier mobility in  $MoS_2$  [32], the lack of air stability in phosphorene and the gapless nature of stanene. Thus, researchers have made efforts to seek for novel 2D materials to achieve more efficient and promising sensing devices. In this regard, doped stanene nanosheets have attracted significant attention for application in semiconductor sensors. Doping different elements into the structure of stanene induces significant

changes in the electronic properties such as band gap opening [33]. Recently, Chen et al. studied the adsorption of small gas molecule on stanene using first principles calculations [34]. Performing DFT calculations, Grag et al. examined the adsorption of NO,  $NO_2$ ,  $N_2O$  and  $NH_3$  molecules on the BN-codoped stanene monolayers, and proposed that BN codoping is conducive to the interaction of stanene with gas molecules [35]. The effects of elemental doping on the electronic structure of stanene based nanostructures, and the adsorption of different molecules were systematically investigated in our previous works [36-42]. Therefore, band gap opening in an intrinsic gapless material such as stanene is an important issue, which can lead to considerable improvements on its sensing properties. The BN-codoped and AIP-codoped stanene systems exhibit semiconductor characteristics due to the band gap opening around the Fermi level. In this paper, we have carried out a systematic DFT study to examine the structural and electronic properties of the adsorption of  $O_3$  molecules on AIP-codoped stanene monolayers. Our DFT results suggest a sizeable band gap opening in AIP-codoped stanene caused by simultaneous induction of electron/hole in the system. Fig. 1 displays a schematic representation of a typical AIP-codoped stanene based gas sensor for

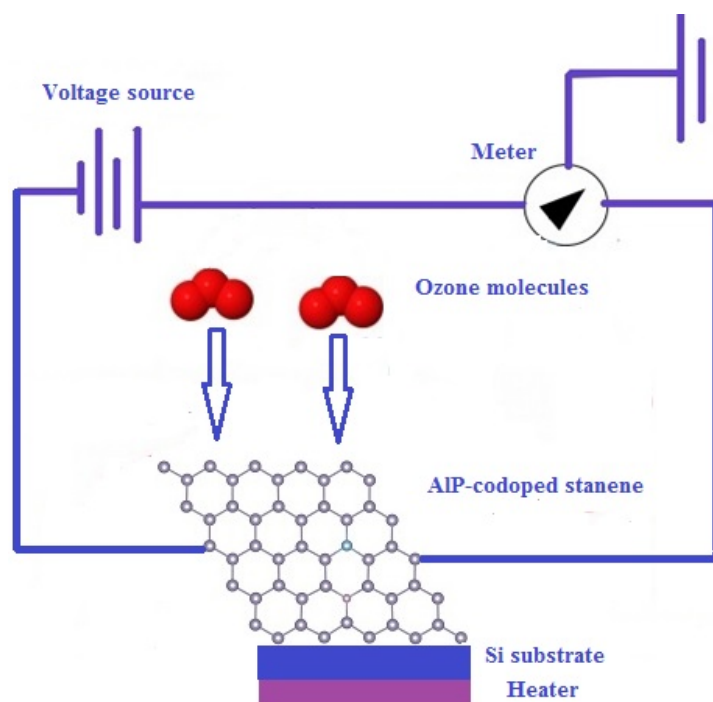


Fig. 1. Schematic representation of an AIP-codoped stanene based gas sensor for ozone detection.

ozone detection. Therefore, our main focus lies on sensing characteristics of the AlP-codoped stanene nanosheets. Mulliken charge analysis reveals a noticeable charge transfer from the stanene system towards ozone molecule. The main aim of this work is to provide theoretical insights into the electronic properties of the AlP-codoped stanene monolayers as highly efficient gas sensors for ozone detection in the environment.

#### COMPUTATIONAL METHODS AND MODELS

The geometry optimization and electronic properties of periodic structures are studied using the density functional theory (DFT) [43, 44], as implemented in the SIESTA code [45]. The generalized gradient approximation (GGA) with the Perdew-Burke-Ernzerhof (PBE) form was used to treat the exchange-correlation functional [46]. The structural models of the considered nanosheets were constructed using the Graphical Display

Interface for Structures, GDIS [47]. The norm-conserving Trouiller-Martins pseudopotential [48] and DZP basis sets for the valence electrons were used in the calculations. The conjugated-gradient optimization of atomic positions was allowed to proceed without any symmetry constraints, while the force was converged within  $0.02 \text{ eV/\AA}$ . We used  $10 \times 10 \times 1$  k-points sampling according to Monkhorst-Pack approach to calculate the total energy and band structure [49]. Also, VESTA program was employed for visualization of the volumetric data such as electron/nuclear densities [50]. At the first step, we have relaxed the atomic positions of the pristine stanene supercell to obtain the optimized structure. A large  $5 \times 5$  supercell ( $23.38 \text{ \AA} \times 23.38 \text{ \AA}$ ) of stanene with a vacuum space of  $20 \text{ \AA}$  in the Z direction was constructed to investigate the effects of  $O_3$  gas molecules on the electronic properties of stanene monolayer. Fig. 2a shows the optimized structure of the pristine

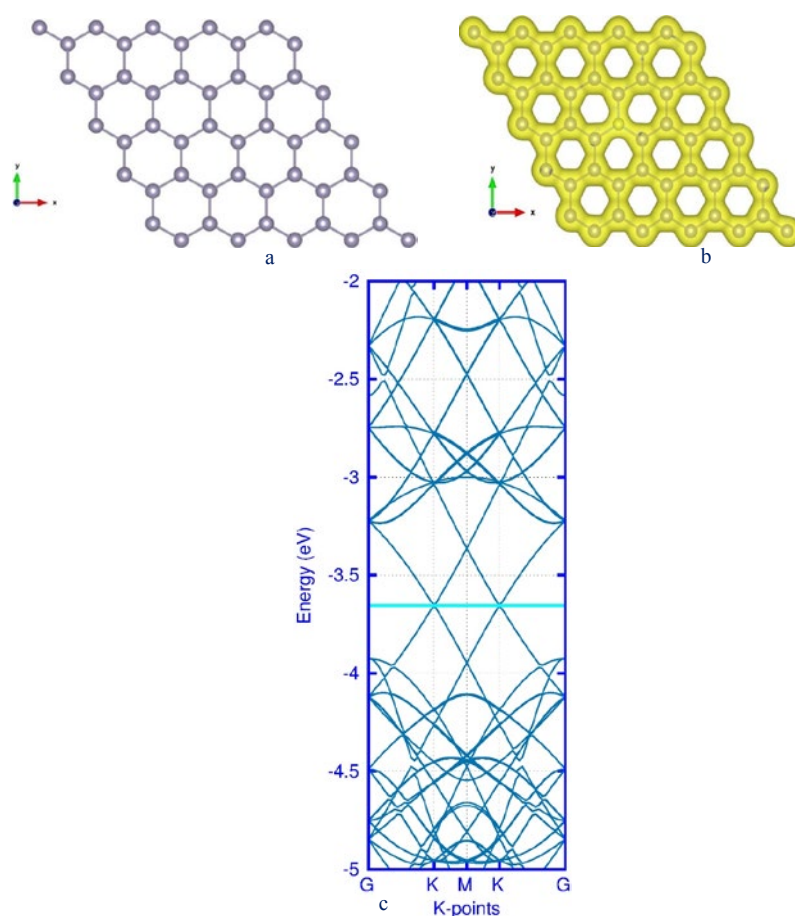


Fig. 2. (a) Top view of the optimized structure of  $5 \times 5 \times 1$  supercell of stanene monolayer, (b) total electron density surface of the pristine stanene monolayer (Isosurface:  $0.03 \text{ e. \AA}^{-3}$ ), and (c) electronic band structure of the pristine stanene monolayer along with the total density of states.

stanene supercell. During the optimization of the structure, all atoms of the system were allowed to relax. The adsorption energy ( $\Delta E_{ad}$ ) of the gas molecule on the stanene monolayer is defined as follows:

$$\Delta E_{ad} = E_{gas-stanene} - E_{gas} - E_{stanene} \quad (1)$$

where  $E_{gas-stanene}$  is the total energy of the stanene monolayer with adsorbed O<sub>3</sub> molecule, while  $E_{gas}$  and  $E_{stanene}$  represent the total energies of the isolated gas molecule and pristine stanene system, respectively.

## RESULTS AND DISCUSSION

### Structural and electronic properties AlP-codoped stanene

In this work, we have considered an initial two-dimensional hexagonal unit cell of stanene containing two tin atoms. After optimization of the whole 5×5 supercell, the Sn-Sn bond length and lattice constant were calculated to be 2.83 Å and 4.67 Å. The calculated results are very close to the previous reports [51, 52]. The bond lengths, bond angles, adsorption energies and charge transfers for O<sub>3</sub> molecule adsorbed on the stanene monolayer were listed in Table 1. The charge density distribution of the whole stanene system was also analyzed in this work. Fig. 2b shows the total electron density profile of the pristine stanene supercell. As can be seen from this Figure, the charges were considerably delocalized over the stanene monolayer. Also, the band structure plot of the pure stanene supercell was depicted in Fig. 2c. As can be seen from this figure, the pristine 5×5 supercell of stanene is a zero band gap material. The substitutional doping of Al and P atoms into the stanene monolayer makes substantial changes in the electronic structure, which results in a band gap opening in the system. Our band structure calculations indicate that Al-P codoping gives rise to an effective band gap

opening and changes the electronic properties in stanene. Recently, codoping of B and N atoms has been experimentally investigated, and found to be beneficial in the graphene for various applications [53, 54]. Important to note is that B/N co-doping induces both the electron and hole, simultaneously [55], thus making a possibility for band gap opening in the system. Fig. 3a shows the optimized structure of the AlP-codoped stanene supercell. In this doping position, the Sn atoms of the same hexagon were replaced by Al and P atoms. The total electron density surface plot of the AlP-codoped stanene (Fig. 3b) shows the accumulation of charge density along the Sn-Al and Sn-P bonds, indicating the formation of covalent bonds. Moreover, we have presented the band structure plot for the AlP-codoped stanene monolayer. Fig. 3c shows the band structure of the mono-Al/P doped stanene sheet before the adsorption process. This figure shows that Al-P codoped stanene system opens the energy gap at the Fermi level. In other words, there is an energy gap between the valence and conduction band edges for the Al-P codoped structure. As can be seen from this Figure, Al/P codoped stanene acts as a semiconductor with a non-zero band gap value. This system can be successfully used for the design and development of semiconductor based devices such as gas sensors. In this figure, we can see that the Fermi level locates between the valence band maximum (VBM) and conduction band minimum (CBM) with a Dirac cone disappeared at the K point. In contrast, in the band structure of the pristine stanene monolayer, we can see the formation of the Dirac cone at the K point. It is well-known to the chemical sensor community that the semiconducting material is required for the sensing characteristics of gas molecules. However, in the case of pristine stanene nanosheet, the system is gapless, and its sensing capability is greatly influenced by its zero band gap. After the inclusion of Al and P atoms in the structure of

Table 1. Bond lengths (Å), angles (in degrees), adsorption energies (in eV) and charge transfers for O<sub>3</sub> molecule adsorbed on the pristine and doped stanene nanosheets.

Configuration	Sn-O	O-O	O-O-O	ΔQ	ΔE <sub>ad</sub>
A	2.18-2.22	1.50-1.55	109	0.705	-1.85
B	2.91	1.41-1.43	117.4	0.465	-0.45
C	2.24-2.29	1.48-1.55	111.1	-0.697	-2.45
D	2.91	1.41-1.43	117.5	-0.456	-0.58
E	2.24-2.27	1.51-1.52	111.1	-0.699	-2.85
F	2.90	1.42-1.43	111.3	-0.468	-0.62
G	2.32	1.43-1.67	111.1	-0.818	-3.24
H	2.21-2.27	1.50-1.53	111.6	-0.708	-3.12
Non-adsorbed		1.28	116.8		

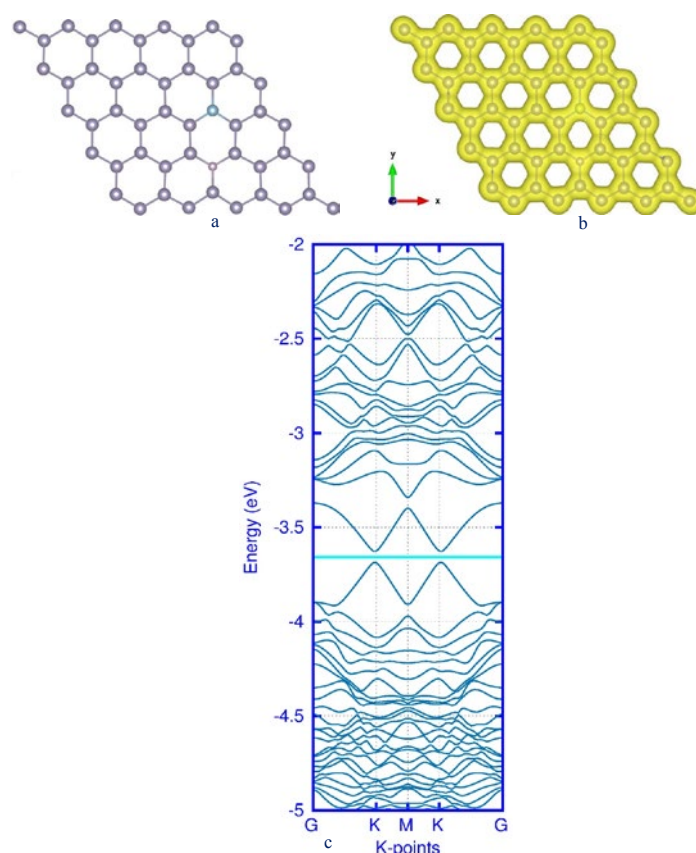


Fig. 3. (a) Optimized structure of AlP-codoped  $5 \times 5 \times 1$  supercell of stanene, (b) top view of the total electron density surface (Isosurface:  $0.03 \text{ e. \AA}^{-3}$ ), (c) Band structure of AlP-codoped stanene monolayer. The Fermi level is indicated by a blue solid line.

stanene, we found a tunable band gap opening in stanene, suggesting its potential applicability for gas sensing materials.

#### *Sensing properties of pristine and doped stanene monolayers*

For the ozone/stanene system, we have investigated various possible adsorption configurations in which the central and side oxygen atoms of the ozone molecule approach to the Sn or doped Al/P atoms of the pristine and doped stanene monolayer. Firstly, we have considered the adsorption of  $O_3$  molecule on the pristine (undoped) stanene monolayer. The optimized geometry configurations of  $O_3$  adsorbed stanene nanosheets were displayed in Fig. 4. For  $O_3$  adsorption on the undoped stanene, only two local minima structures were obtained upon the relaxation process. In one configuration (configuration A),  $O_3$  molecule locates above the stanene surface and the side oxygen atoms of  $O_3$  are positioned to the tin atoms. In this configuration, strong chemical bonds were formed between the

tin and oxygen atoms. In configuration B, the central oxygen atom of the  $O_3$  molecule locates above the stanene sheet with a distance of  $2.91 \text{ \AA}$ . The total electron density plots of configurations A and B were also displayed in Fig. 4. This figure clearly shows the charge accumulation between the tin and side oxygen atoms of the  $O_3$  molecule, indicating the formation of Sn-O chemical bonds. In contrast, it can be seen from electron density plot of configuration B that there is a charge depletion between the central oxygen atom of the  $O_3$  molecule and tin atom. This reveals the physical nature of the adsorption with the higher adsorption distance of  $2.91 \text{ \AA}$ . After the adsorption process, the O-O bonds of the adsorbed molecule were significantly elongated because of the transfer of electronic density from the stanene and O-O bonds to the newly formed Sn-O bonds. In the case of  $O_3$  molecule on the Al-doped and P-doped stanene monolayers, the optimized structures were shown in Figs. 5 and 6, respectively. Similarly, configurations C and E represent the interaction

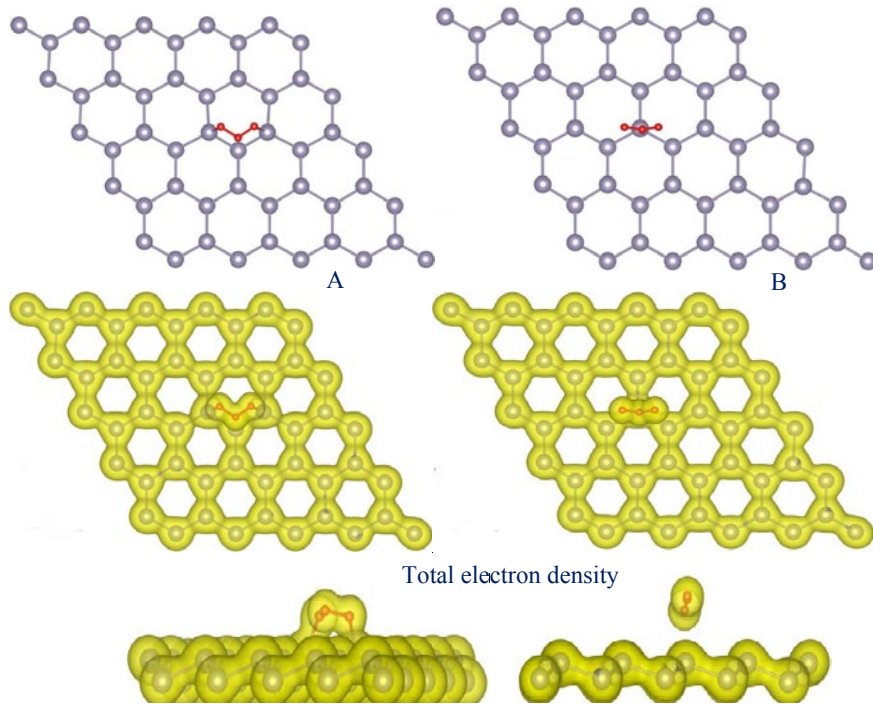


Fig. 4. Optimized structures of the adsorption of  $O_3$  molecule on the pristine stanene monolayer along with the total electron density plots (Isosurface:  $0.03 e. \text{\AA}^{-3}$ ). In configuration A, the side oxygen atoms of the  $O_3$  molecule interact with the Sn atoms of the pristine stanene, and in configuration B, the central oxygen atoms of the  $O_3$  molecule shows an interaction with the Sn atom.

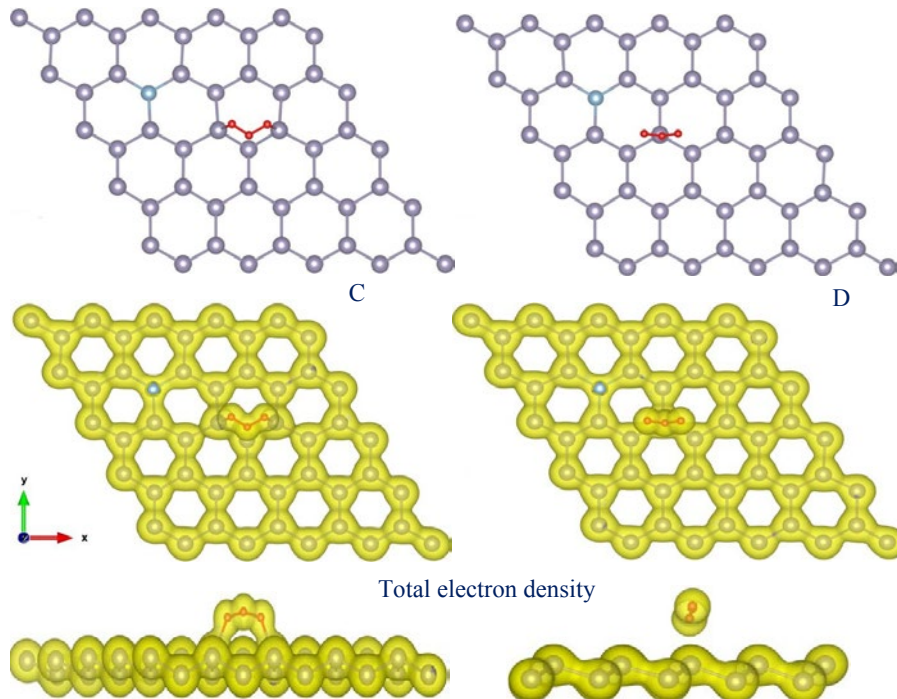


Fig. 5. Optimized structures of the adsorption of  $O_3$  molecule on the Al-doped stanene monolayer along with the total electron density plots (Isosurface:  $0.03 e. \text{\AA}^{-3}$ ). Configuration C represents the interaction between side oxygen atoms of  $O_3$  molecule and Sn atoms on the Al-doped stanene, while configuration D shows the interaction between central oxygen and Sn atom.

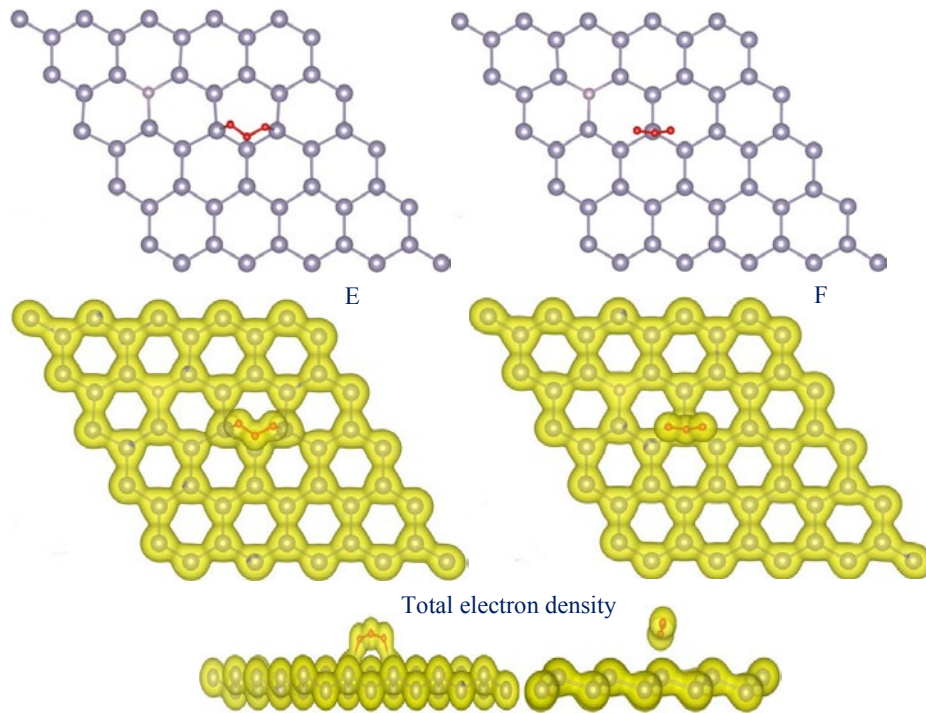


Fig. 6. Optimized structures of the adsorption of O<sub>3</sub> molecule on the P-doped stanene monolayer along with the total electron density plots (Isosurface: 0.03 e. Å<sup>-3</sup>). Configuration E represents the interaction between side oxygen atoms of O<sub>3</sub> molecule and Sn atoms on the P-doped stanene, while configuration F shows the interaction between central oxygen and Sn atom on the stanene surface.

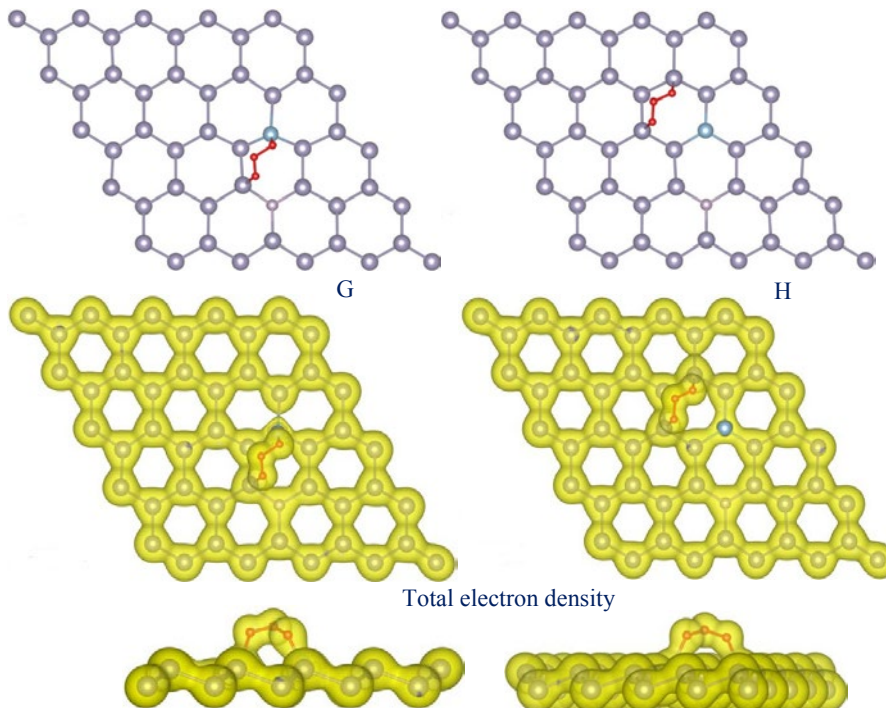


Fig. 7. Optimized structures of the adsorption of O<sub>3</sub> molecule on the AlP-codoped stanene monolayer along with the total electron density plots (Isosurface: 0.03 e. Å<sup>-3</sup>). Configuration G represents the binding of the side oxygen atoms of O<sub>3</sub> molecule to the Sn and Al atoms of AlP-doped stanene monolayer, while configuration H shows the binding of the oxygen atoms to the two Sn atoms of AlP-codoped stanene system.

of the side oxygen atoms of the O<sub>3</sub> molecule with the stanene, while D and F show the interaction between the central oxygen atom and stanene sheet. The electron density plots in Figs. 5 and 6 show that the electronic density distribute along the newly formed Sn-O bonds. In the case of O<sub>3</sub> adsorption through its central oxygen site, there is no charge distribution between the oxygen and tin atom. The adsorption of O<sub>3</sub> molecule on the AlP-codoped stanene monolayer was also displayed in Fig. 7. In configuration H, the side oxygen atoms interact with the tin atoms of the AlP-codoped stanene, and configuration G presents the interaction of O<sub>3</sub> molecule above the Al-site. In this configuration, a new Al-O bond (1.84 Å) was formed between the doped stanene and O<sub>3</sub> molecule. It can be seen from this figure that the O<sub>3</sub> molecule preferentially interacts with the stanene monolayer by its side oxygen atoms. In this case, the chemical nature of the adsorption was also confirmed by the

provided electron density plots, which show the concentration of the electron density along the newly formed Sn-O bonds between stanene and O<sub>3</sub> molecule.

In order to fully examine O<sub>3</sub> adsorption on the AlP-codoped stanene monolayer, we have calculated the adsorption energies for the stable configurations (see Table 1). The results suggest that the adsorption of O<sub>3</sub> molecule on the doped stanene monolayer is more energetically favorable than that on the pristine one. Thus, O<sub>3</sub> adsorption on the codoped AlP+stanene system is more energetically favored. Important to note is that, on the AlP-codoped stanene, the process is more favorable in energy than that on the mono-AlP doped and pristine stanene. This can be attributed to the better semiconductor characteristics of the AlP-codoped stanene, which opens a band gap due to the simultaneous induction of electron/hole in the system. As a result, we found that

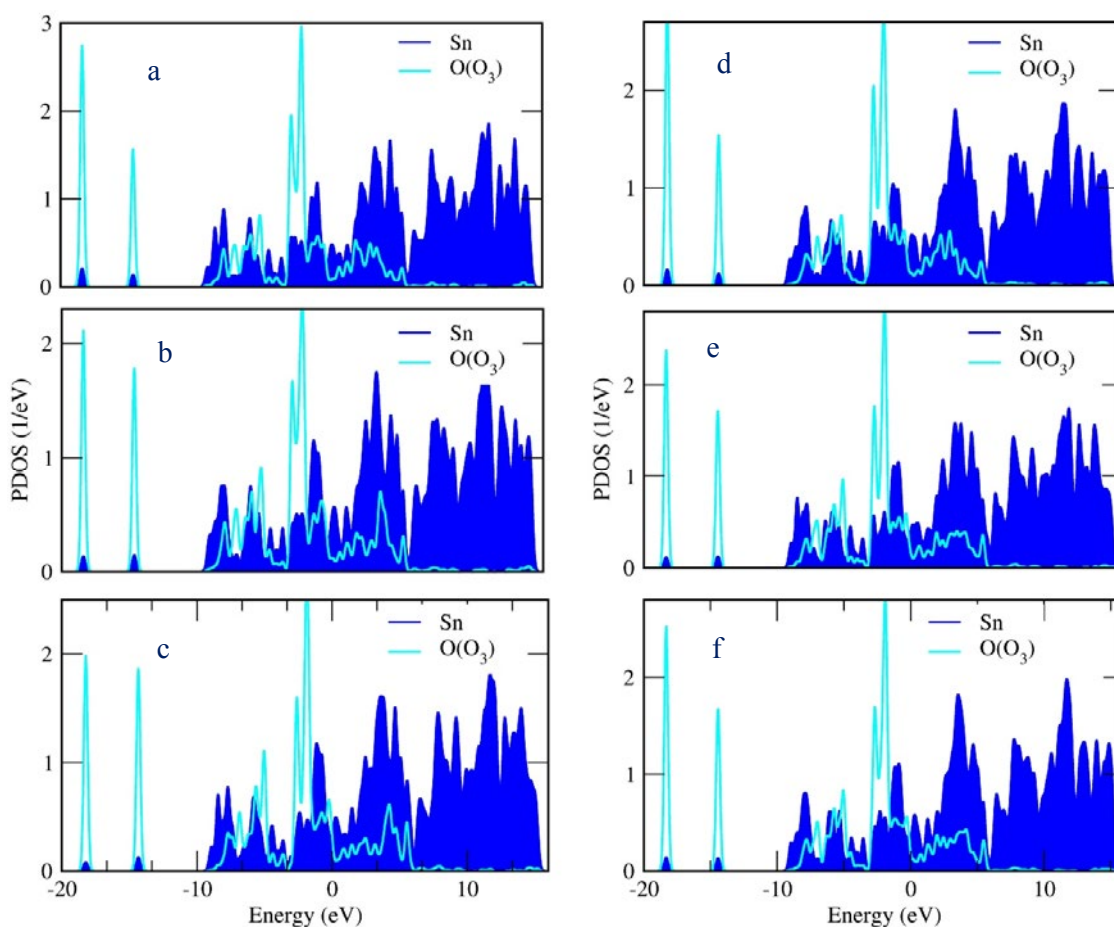


Fig. 8. Projected density of states of the Sn and O atoms for O<sub>3</sub> molecule adsorption on the pristine and doped stanene monolayers. (a, b) PDOS plots for configuration A, and (c, d) PDOS plots for configuration C, (e, f) PDOS plots for configuration E.

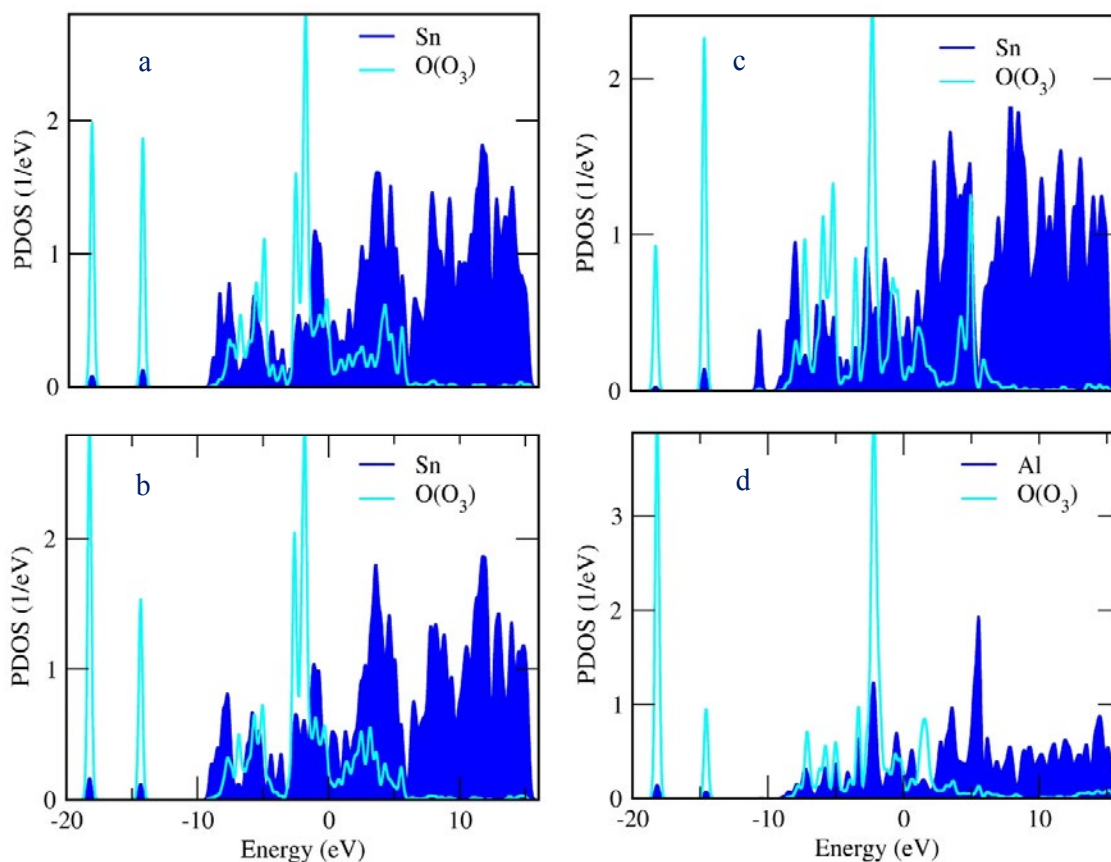


Fig. 9. Projected density of states (PDOS) of the Sn and O atoms for O<sub>3</sub> molecule adsorption on the pristine and doped stanene monolayers, (a, b) represent the PDOS plots for configuration H, and (c, d) show those for configuration G.

Al-P pair doping improves adsorption energy and shows higher sensitivity and adsorption capability towards ozone molecules.

Mulliken charge analysis reveals a noticeable charge transfer (about -0.818 e) from the AlP-codoped stanene to the O<sub>3</sub> molecule. In order to investigate the changes in the electronic properties of the adsorption system, we have presented the projected density of states (PDOS) profiles. The relevant PDOS spectra for O<sub>3</sub> adsorption on the pristine and doped stanene monolayers were shown in Figs. 8 and 9. Fig. 8 shows the PDOS spectra for O<sub>3</sub> adsorption on the pristine, Al-doped and P-doped stanene, and Fig. 9 shows the PDOS profiles for adsorption on the AlP-codoped system. It can be seen from Fig. 8 that there are significant overlaps between the PDOS spectra of the tin and side oxygen atoms, representing the formation of chemical bonds between them. The formation of chemical Sn-O and Al-O bonds was also evidences by the PDOS profiles of these atoms in Fig. 9. Hence, AlP codoping is conducive to

the interaction between stanene and O<sub>3</sub> molecule. The charge density difference (CDD) plots of the O<sub>3</sub> adsorbed Al-doped stanene monolayers were shown in Fig. 10. As can be seen from the CDD plot of configuration C, the electronic density increases at the middle of the Sn atoms of stanene monolayer and side oxygen atoms, indicating the formation of chemical bonds between these atoms. Our results indicate that the charges were accumulated on the adsorbed O<sub>3</sub> molecule. The CDD profile of configuration D shows that the central oxygen atom of O<sub>3</sub> molecule weakly interacts with the stanene monolayer. This implies that the interaction of O<sub>3</sub> molecule with stanene through its central oxygen atom is a physisorption process. As a result, by considering the CDD profiles, we concluded that the charges were mainly accumulated on the adsorbed gas molecule. The chemical nature of the adsorption was also confirmed by the CDD plots and PDOS analysis. We have also performed the band structure calculations for the doped stanene monolayers

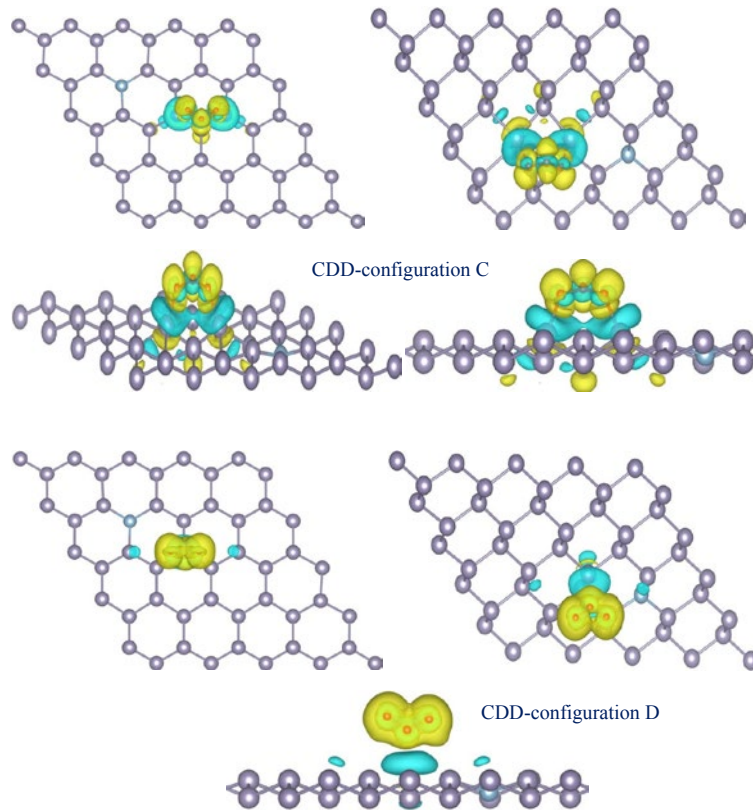


Fig. 10. Isosurface plots of the electron charge density difference for  $O_3$  adsorbed Al-doped stanene monolayers with the isovalue of  $\pm 0.001$  a.u. The cyan and yellow colors represent the negative and positive charge areas, respectively. The isosurface plots were obtained for configurations C and D in different views.

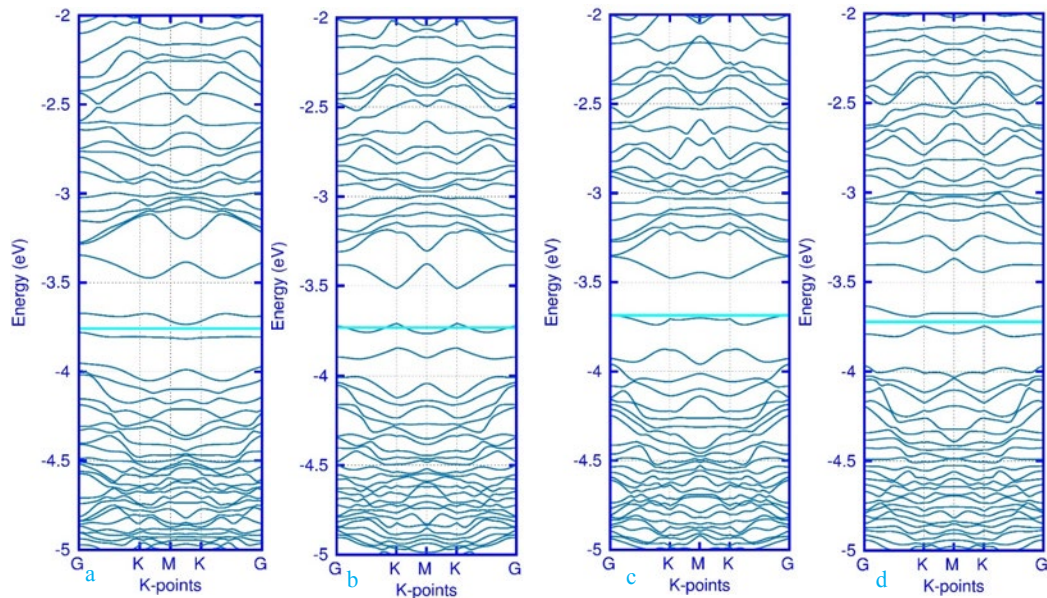


Fig. 11. Band structure plots for  $O_3$  adsorbed stanene monolayers. (a) Band structure plot for pristine stanene monolayer with adsorbed  $O_3$  molecule (configuration A), (b) band structure for P-doped stanene monolayer with adsorbed  $O_3$  (configuration E), (c) band structure for P-doped stanene monolayer with adsorbed  $O_3$  (configuration F) and (d) band structure for AlP-codoped stanene monolayer with adsorbed  $O_3$  (configuration H). The Fermi level is indicated by a dashed solid line

after the adsorption of O<sub>3</sub> gas molecules. The band structure plots were presented in Fig. 11. As can be seen, the position of Fermi level changes after the adsorption process, which leads to some variations on the conductivity of the system. Furthermore, the Dirac cone was completely vanished compared to the perfect stanene sheet. The band structure of the Al/P doped stanene monolayer after the adsorption of O<sub>3</sub> molecule was also represented in Fig. 11d. As can be seen, after the adsorption process, the Dirac cone completely disappears, and the system remains still semiconductor with a Fermi level located between VBM and CBM. The other difference is the shift in the position of Fermi level after the adsorption process compared the Fermi level position in the band structure of Al/P doped stanene without any adsorbed O<sub>3</sub> molecule.

## CONCLUSIONS

The adsorptions of O<sub>3</sub> molecule on the pristine and AlP-codoped stanene sheets were theoretically investigated by using density functional theory calculations. The results showed that the adsorption of O<sub>3</sub> molecule through its side oxygen atoms on the surface gives rise to the formation of chemical bonds between the stanene and O<sub>3</sub> molecule, whereas the adsorption through the central oxygen atom does not provide a chemical bond. After the adsorption, the O-O bonds of the adsorbed O<sub>3</sub> molecule were elongated. Mulliken charge analysis reveals a charge transfer from the stanene to the adsorbed O<sub>3</sub> molecule. O<sub>3</sub> adsorption on the Al-site of AlP-codoped stanene monolayer is more energetically favorable than that on the pristine one. The AlP-codoped stanene exhibits better sensing capability due to its semiconductor characteristics. The reason can be attributed to the simultaneous AlP codoping, which induces both electron/hole in the system and opens a sizeable band gap in the system. Therefore, the adsorption of O<sub>3</sub> molecule on the AlP-codoped structure is more energetically favored. The projected density of states show the formation of chemical bonds between the side oxygen atoms of the O<sub>3</sub> molecule and tin atoms. Moreover, the charge density difference calculations indicate the charge accumulation on the adsorbed O<sub>3</sub> molecule.

## ACKNOWLEDGEMENT

This work has been supported by Azarbaijan Shahid Madani University.

## CONFLICT OF INTEREST

The authors declare that there is no conflict of interests regarding the publication of this manuscript.

## REFERENCES

- [1] K. Novoselov, A.K. Geim, S. Morozov, D. Jiang, M. Katsnelson, I. Grigorieva, S. Dubonos, A. Firsov, *Nature*, 438, 197 (2005).
- [2] N. Drummond, V. Zolyomi, V. Fal'Ko, *J. Phys. Rev. B*, 85, 075423 (2012).
- [3] W. Hu, N. Xia, X. Wu, Z. Li, J. Yang, *Phys. Chem. Chem. Phys.*, 16, 6957 (2014).
- [4] W. Hu, X. Wu, Z. Li, J. Yang, *Nanoscale*, 5, 9062 (2013).
- [5] W. Xia, W. Hu, Z. Li, J. Yang, *Phys. Chem. Chem. Phys.*, 16, 22495 (2014).
- [6] T.P. Kaloni, *J. Phys. Chem. C*, 118, 25200 (2014).
- [7] M. Zhao, X. Zhang, L. Li, *Sci. Rep.*, 5, 16108 (2015).
- [8] O.U. Aktürk, E. Aktürk, S. Ciraci, *J. Phys. Rev. B*, 93, 035450 (2016).
- [9] A.L. Elias, N. Perea-López, A. Castro-Beltrán, A. Berkdemir, R. Lv, S. Feng, A.D. Long, T. Ha yashi, Y.A. Kim, M. Endo, *Acs Nano*, 7, 5235 (2013).
- [10] L. Chu, H. Schmidt, J. Pu, S. Wang, B. Özyilmaz, T. Takenobu, G. Eda, *Sci. Rep.* 4 7293 (2014).
- [11] J. Qiao, X. Kong, Z.X. Hu, F. Yang, W. Ji, *Nat. Commun.*, 5, 4475 (2014).
- [12] S. Balendhran, S. Walia, H. Nili, S. Sriram, M. Bhaskaran, *Small*, 11, 640 (2015).
- [13] H. Liu, A.T. Neal, Z. Zhu, Z. Luo, X. Xu, D. Tománek, P.D. Ye, *ACS Nano*, 8, 4033 (2014).
- [14] Z. Zhu, D. Tománek, *Phys. Rev. Lett.*, 112, 176802 (2014).
- [15] M. Pumera, *Energy Environ. Sci.*, 4, 668-674 (2011).
- [16] Y. Cai, G. Zhang, Y.W. Zhang, *L. Sci. Rep.*, 4, 6677 (2014).
- [17] X. Yang, C. Cheng, Y. Wang, L. Qiu, D. Li, *Science*, 341, 534 (2013).
- [18] A.K. Singh, K. Mathew, H.L. Zhuang, R.G. Hennig, *J. Phys. Chem. Lett.*, 6 1087 (2015).
- [19] S. Cao, J. Low, J. Yu, M. Jaroniec, *Adv. Mater.*, 27, 2150 (2015).
- [20] G. Fiori, F. Bonaccorso, G. Iannaccone, T. Palacios, D. Neumaier, A. Seabaugh, S.K. Banerjee, L. Colombo, *Nat. Nanotechnol.*, 9, 768 (2014), 9.
- [21] H. Liu, Y. Du, Y. Deng, D.Y. Peide, *Chem. Soc. Rev.*, 44, 2732 (2015).
- [22] X. Chen, C. Tan, Q. Yang, R. Meng, Q. Liang, J. Jiang, X. Sun, T. Ren, *Phys. Chem. Chem. Phys.*, 18, 16229 (2016).
- [23] X. Chen, R. Meng, J. Jiang, Q. Liang, Q. Yang, C. Tan, X. Sun, S. Zhang, T. Ren, *Phys. Chem. Chem. Phys.*, 18, 16302 (2016).
- [24] F- F. Zhu, W- J. Chen, Y. Xu, C - L. Gao, D- D. Guan, C- H. Liu, D. Qian, S- C. Zhang, and J- F. Jia, *Nat. Mater.*, 14, 1020 (2015).
- [25] J. Gao, G. Zhang, Y- W. Zhang, *Sci. Rep.*, 6, 29107 (2016).
- [26] Y. Shaidu, O. Akin-Ojo, *Chem. Phys. Lipids*, 44, 149 (2015).
- [27] O. Leenaerts, B. Partoens, F. Peeters, *Phys. Rev. B*, 77, 125416 (2008).
- [28] F. Schedin, A.K. Geim, S.V. Morozov, E. W. Hill, P. Blake, M.I. Katsnelson, et al. , *Nat. Mater.*, 6, 625 (2007).
- [29] F. K. Perkins, A.L. Friedman, E. Cobas, P. Campbell, G.

- Jernigan, B.T. Jonker, Nano letters, 3, 668 (2013).
- [30] L. Kou, T. Frauenheim, C. Chen, J. Phys. Chem. Letts., 5, 2675 (2014).
- [31] Y Cai, Q. Ke, G. Zhang, Y.W. Zhang, J. Phys. Chem. C, 119(6), 3102 (2015).
- [32] B. Radisavljevic, A. Radenovic, J. Brivio, I.V. Giacometti, A. Kis, Nat. Nanotechnol., 6(3), 147 (2011).
- [33] P. Garg, I. Choudhuri, A. Mahata, B. Pathak, Phys. Chem. Chem. Phys., 19, 3660 (2017).
- [34] X. Chen, C. Tan, Q. Yang, R. Meng, Q. Liang, M. Cai, S. Zhang, J. Jiang, J. Phys. Chem. C, 120(26), 13987 (2016).
- [35] P. Garg, I. Choudhuri, B. Pathak, Phys. Chem. Chem. Phys., 19, 31325 (2017).
- [36] A. Abbasi, Physica E: Low-dimensional Systems and Nanostructures, 108, 34 (2019).
- [37] A. Abbasi, J.J. Sardroodi, Appl. Surf. Sci., 456, 290 (2018).
- [38] A. Abbasi, J.J. Sardroodi, Physica E: Low-dimensional Systems and Nanostructures, 108, 34 (2019).
- [39] A. Abbasi, Synthetic Metals, 247, 26 (2019).
- [40] A. Abbasi, J.J. Sardroodi, J. Appl. Phys., 124, 165302 (2018).
- [41] A. Abbasi, J.J. Sardroodi, Adsorption, 24, 443 (2018).
- [42] A. Abbasi, J.J. Sardroodi, A.R. Ebrahimzadeh, M. Yaghoobi, Appl. Surf. Sci., 435, 733 (2018).
- [43] P. Hohenberg, W. Kohn, Phys. Rev. B, 136, B64 (1964).
- [44] W. Kohn, L. Sham, Phys. Rev. B, 140, A1133 (1965).
- [45] J.M. Soler, E. Artacho, J.D. Gale, A. Garcia, J. Junquera, P. Ordejón, D. Sánchez-Portal, J. Phys. Condens. Matter, 14, 2745 (2002).
- [46] J.P. Perdew, K. Burke, M. Ernzerhof, Phys. Rev. Letts., 78, 1396 (1981).
- [47] A. Koklj, Comput. Mater. Sci., 28, 155 (2003).
- [48] N. Troullier, J. Martins, Phys. Rev. B, 43, 1993 (1991).
- [49] H.J. Monkhorst J.D. Pack, Phys. Rev. B, 13, 5188 (1976).
- [50] K. Momma F. Izumi, J. Appl. Crystallogr., 44, 1272 (2011).
- [51] B. Broek, M. Houssa, E. Scalise, G. Pourtois and V. V. Afanas'ev Stesmans, 2D Materials, 1, 021004 (2014).
- [52] Y. Xu, B. Yan, H. J. Zhang, J. Wang, G. Xu, P. Tang, W. Duan, S.C. Zhang, Phys. Rev. Lett., 111, 136804 (2013).
- [53] A. Jafari, M. Ghoranneviss A.S. Elahi, J. Cryst. Growth., 438, 70 (2016).
- [54] D. Wei, Y. Liu, Y. Wang, H. Zhang, L. Huang, G. Yu, Nano Lett., 9, 1752 (2009).
- [55] I. Choudhuri, N. Patra, A. Mahata, R. Ahuja, B. Pathak, J. Phys. Chem. C, 119, 24827 (2015).